

Article

Electromechanical Natural Frequency Analysis of an Eco-Friendly Active Sandwich Plate

Rasool Moradi-Dastjerdi  and Kamran Behdinin *

Advanced Research Laboratory for Multifunctional Lightweight Structures (ARL-MLS),
Department of Mechanical and Industrial Engineering, University of Toronto, Toronto, ON M5S 3G8, Canada
* Correspondence: behdinin@mie.utoronto.ca

Abstract: In conventional piezoelectric ceramics, their brittle nature and containing lead are two crucial issues that significantly restrict their uses in many applications such as biomedical devices. In this work, we suggest the use of an eco-friendly piezoelectric nanocomposite material to piezoelectrically activate a cantilever meta-structure plate to be used as a novel actuator/sensor or even energy harvester; this cantilever plate is formed of several polymeric links to create an auxetic core plate that structurally shows a negative Poisson's ratio. Moreover, the active nanocomposite materials are used as the face sheets on the auxetic plate; these active layers are made of nanowires of zinc oxide (ZnO) that are placed into an epoxy matrix in different forms of functionally graded (FG) patterns. For such active sandwich plates (ASPs) with potential electromechanical applications, a coupled electromechanical analysis has been performed to numerically investigate their natural frequencies as a crucial design parameter in such electromechanical devices. By developing a meshless method based on a higher plate theory, the effects of nanowire volume fraction, nanowire distribution, auxetic parameters, layer dimensions, and electrical terminal set-up have been studied; this in-depth study reveals that ASPs with an auxetic core have much lower natural frequencies than ASPs with honeycomb cores which would be very helpful in designing actuators or energy harvesters using the proposed cantilever sandwich plates.

Keywords: electromechanical vibrations; active sandwich plates; auxetic plate; piezoelectric zinc oxide nanowire; eco-friendly piezoelectric materials



Citation: Moradi-Dastjerdi, R.; Behdinin, K. Electromechanical Natural Frequency Analysis of an Eco-Friendly Active Sandwich Plate. *Actuators* **2022**, *11*, 261. <https://doi.org/10.3390/act11090261>

Academic Editor: Shuxiang Dong

Received: 18 August 2022

Accepted: 6 September 2022

Published: 9 September 2022

Publisher's Note: MDPI stays neutral with regard to jurisdictional claims in published maps and institutional affiliations.



Copyright: © 2022 by the authors. Licensee MDPI, Basel, Switzerland. This article is an open access article distributed under the terms and conditions of the Creative Commons Attribution (CC BY) license (<https://creativecommons.org/licenses/by/4.0/>).

1. Introduction

Recently, due to the high demand for self-powered electronic devices, researchers from both academia and industry are becoming more interested in active structures. Among the newly introduced active structures, those activated with piezoelectric materials have gained more attention due to their real-time conversion of electrical potential to mechanical deflections or vice versa [1]. Another reason for the popularity of this material is the fast development of electronic devices; this development makes those devices miniaturized with fewer electric power needs indeed, therefore generating that power using piezoelectric is becoming more feasible [2–4]. The technology of the Internet of Things (IoT) is a promising example of such an electronic devices that needs a set of self-powered sensors and actuators to provide real-time sensing or actuating signals [5,6]. The required energy to power such electronics can be obtained using piezoelectric effects. However, the conventional, widely used piezoceramics have various disadvantages, such as their brittle nature and containing a toxic material (i.e., lead) [7,8]; these issues with lead-based piezoceramics have motivated scientists to propose alternatives such as piezoelectric nanocomposites which eliminate toxic materials [9–11]; it was found that ZnO fibers as an eco-friendly piezoelectric material perform greater at nanoscales in comparison with their bulk sizes [12–14]. Hence, the mixture of nanoscale ZnOs and a passive/active polymer are examined to be substituted for conventional brittle and lead-based piezoceramics. The resulting piezoelectric

nanocomposite brings some other benefits to the final electronic device, including structural weight reduction and biocompatibility [15,16]. However, the broader application of such piezoelectric nanocomposites needs extensive knowledge of their electromechanical behaviours [17,18]. Given their applications as actuators, sensors, nanogenerators, or energy harvesters, the demands for modal analysis of piezoelectrically activated structures are brighter [19–21].

With the successful application of nanocomposite materials in introducing multifunctional structures, it has been demonstrated that the use of such material leads to significant improvements in the mechanical behaviour of the resulting structures [22–27]. Carbon nanotube, graphene, and nanoclay reinforced nanocomposite materials are the three most highlighted nanofillers among the passive nanoscale reinforcements [28–34]. The use of nanocomposites reinforced with one or a combination of these passive nanofillers in a nanocomposite structure would improve natural frequencies of that structure [35–37]. However, recently, the use of biocompatible and eco-friendly piezoelectric nanofillers such as ZnO, gallium nitride, or barium titanate has also been considered. For example, bimorph polymeric plates with embedded ZnO or gallium nitride nanowires were suggested in [38] where the static and vibration behaviour of such piezoelectrically activated plates were compared. Mossalaei et al. [11] proposed piezoelectric PVDF cylindrical shells with embedded piezoelectric nanotubes of boron nitride; they presented torsional buckling resistance of such shells in a framework of a coupled thermo-electromechanical study. Moreover, to propose active lightweight panels, a polymeric foam plate has been considered in between two polymeric face sheets with embedded ZnO nanowires [39,40]. For such piezoelectric sandwich plates, the mechanical and thermal buckling stability behaviours were reported. Electromechanical characterization of piezoelectric nanocomposite materials with embedded nanoscale ZnO that can be used as a nanogenerator were presented in [41,42]. Arshid et al. [43] proposed the use of piezoelectric PVDF nanoplates reinforced with carbon nanotubes in FG patterns; they also presented the buckling stability of such eco-friendly nanoplates. Moreover, various application-oriented devices made of advanced materials have been introduced, where the use of eco-friendly piezoelectric materials is highlighted. To mention some, pure PVDF and PVDF-TrFE as piezoelectric polymers were utilized to propose inexpensive and wearable energy harvesters with biomedical applications [44,45]. To introduce a biocompatible insulin micropump, Angelou et al. [46] successfully proposed the use of a piezoelectrically activated diaphragm made of PVDF/barium titanate. Cantilever-type energy harvesters with a point mass made of a mixture of PVDF/aluminum nitride were also proposed to convert mechanical vibration energies to electrical one [47,48]. Moreover, a cantilever passive polymeric beam with embedded ZnO nanowires were proposed for harvesting energies from low-frequency vibrations of a human body and powering a temperature sensor [49].

However, in this work, a novel lightweight active sandwich plate is suggested to eliminate the concerns with structures/devices that contain PZT-based piezoelectric materials. Due to the use of an auxetic polymeric core and piezoelectric ZnO nanowire-reinforced face sheets, the resulting ASP is also lightweight and eco-friendly; this ASP is considered as a cantilever plate to be used as an actuator, sensor, or energy harvester. To improve the performance of the ASP, FG patterns have been employed for the dispersion of nanowires in the face sheets. Therefore, the newly proposed ASP is not only an eco-friendly multifunctional structure, but is also lightweight structure. As an essential design parameter for the potential electromechanical applications of the proposed ASP, the vibrational behaviour of the ASP has been characterized by evaluating the effects of nanowire content and distribution, auxetic parameters, ASP dimensions, and electrical terminal set-ups. To do so, a meshless solution incorporated with Reddy's higher plate theory with only five unknowns and MLS shape functions has been developed. To impose the effect of supports, the transformation matrix has been used to avoid penalty parameters employed in the element-free Galerkin method. Therefore, the combination of the developed meshless

solution and the utilized plate theory is expected to offer a computationally cost-effective procedure while the accuracy level of results is still high.

2. Modeling of the Structure

As described before, a novel active sandwich structure which includes a cantilever auxetic plate sandwiched by two eco-friendly piezoelectric nanocomposite layers with potential applications as a sensor/actuator or energy harvester is proposed in this study as illustrated in Figure 1; it is assumed that the inner surfaces of the piezoelectric layers are grounded while the outer ones are electrically free or connected to a receiver (in sensor or energy harvester applications) or an electrical source (in actuator applications). Moreover, as shown in Figure 2, there are four geometrical design dimensions including l_x , h_x , t_x and θ in auxetic structures; it should be mentioned that since the thickness of the ASP is well-smaller than length and width of the ASP, a plate model has been considered so normal stress along the thickness of the plate (σ_{zz}) is negligible. Moreover, it is assumed that the face sheets are perfectly attached (no slip) to auxetic core. Furthermore, a linear voltage variation through the thickness of face sheets has been assumed.

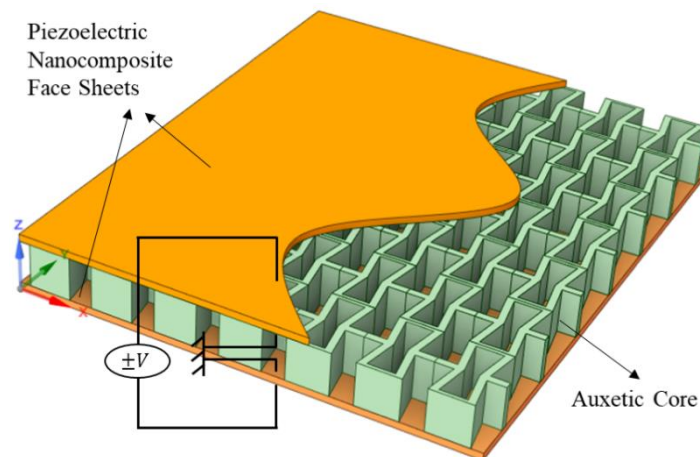


Figure 1. Schematic design of the cantilever ASP with an auxetic core and two thinner face sheets.

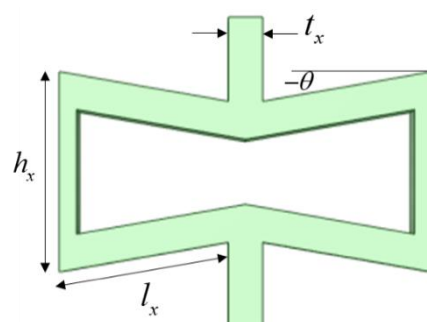


Figure 2. A unit cell of the auxetic core pattern with its geometrical parameters.

2.1. Material Properties

As stated before, the middle cellular layer is made of a polymeric material with an auxetic unit cell shape; this specific type of unit cell dedicates negative Poisson's ratio to the structural behaviour of the middle layer. The geometrical shape of such structures can be described by utilizing the inclined angle θ , the ratio of cell wall length $\alpha_x = h_x/l_x$, and the slenderness ratio of the unit cell wall $\beta_x = t_x/l_x$. Using these shape parameters and the material properties of the employed material, the density ρ^c , Poisson's ratio ν^c , and the

shear G^c and Young's E^c moduli of an auxetic unit cell and generally the middle layers are estimated as follows [50]:

$$E_{11}^c = E(\beta_x)^3 \frac{\cos \theta}{(\alpha_x + \sin \theta) \sin^2 \theta}, \quad E_{22}^c = E(\beta_x)^3 \frac{(\alpha_x + \sin \theta)}{\cos^3 \theta} \quad (1)$$

$$G_{12}^c = E(\beta_x)^3 \frac{(\alpha_x + \sin \theta)}{(\alpha_x)^2 (1 + 2\alpha_x) \cos \theta}, \quad G_{13}^c = G\beta_x \frac{\cos \theta}{(\alpha_x + \sin \theta)}, \quad (2)$$

$$G_{23}^c = G\beta_x \frac{(1 + 2\sin^2 \theta)}{2\cos \theta (\alpha_x + \sin \theta)}$$

$$\nu_{12}^c = \frac{\cos^2 \theta}{(\alpha_x + \sin \theta) \sin \theta} \quad (3)$$

$$\rho^c = \rho \frac{\beta_x (\alpha_x + 2)}{2\cos \theta (\alpha_x + \sin \theta)} \quad (4)$$

where ρ , ν , G and E show the material properties of the polymeric material used for the middle layer; it should be mentioned that for the negative values of inclined angle θ , the Poisson's ratio of the middle layer ν_{12}^c would be negative.

Regarding the active layers of the sandwich plates, it is assumed that the nanowires of ZnO are dispersed into the polymeric matrix in FG patterns to improve the functionality of the overall structure. To estimate the overall electromechanical properties of such piezoelectric nanocomposite, a closed-form coupled model that uses a linear piezoelectric theory were utilized [10]; this model was verified by finite element simulations in [10]. In this work, the profiles of nanowire distribution in the z direction of outer layers can be determined using the following equations [51]:

$$\text{Top skin layer : } f_r(z) = [1 + (2z - t)/2t_p]^p f_0 \quad (5)$$

$$\text{Bottom skin layer : } f_r(z) = [1 - (2z + t)/2t_p]^p f_0 \quad (6)$$

where f_r and f_0 are ZnO nanowire volume fractions along in z direction and at the outer surfaces. In addition, p is a number called exponent value that can control the distribution of nanowires.

2.2. Governing Equations

For such APSs in electromechanical environments, the weak form of the equation of motion is described as follows [52]:

$$\int_V [\rho(z) \ddot{\mathbf{d}}_t \cdot \delta \mathbf{d}_t + \boldsymbol{\sigma} \cdot \delta \boldsymbol{\varepsilon} - \mathbf{D} \cdot \delta \mathbf{E}] d\Omega = 0 \quad (7)$$

where $\mathbf{d}_t = \{u \ v \ w\}^T$ is the displacement vector of the structure along a Cartesian coordinate system. Moreover, $\boldsymbol{\sigma}$, \mathbf{D} , $\boldsymbol{\varepsilon}$ and \mathbf{E} are vectors of mechanical stress, electrical displacement, mechanical strain and electric field, respectively. Furthermore, V is the volume of the APSs.

In this work, the displacement field of these APSs is defined using a five-unknown higher-order theory introduced by Reddy as follows [53]:

$$\begin{aligned} u &= u_0(x, y) + z\theta_x(x, y) + z^3 c_1 (\theta_x + w_{0,x}) \\ v &= v_0(x, y) + z\theta_y(x, y) + z^3 c_1 (\theta_y + w_{0,y}) \\ w &= w_0(x, y) \end{aligned} \quad (8)$$

where the constant is defined as $c_1 = -4/3t^2$ and the subscript 0 is used for showing the mid-plane deflections. Moreover, θ_x and θ_y are mid-plane rotations.

Accordingly, the linear in- and out-of-plane strain vectors (i.e., ϵ_b and γ) of the such APSs can be as [53]:

$$\epsilon_b = \epsilon_0 + z\epsilon_1 + c_1z^3\epsilon_3 \quad , \quad \gamma = (1 + 3c_1z^2)\gamma_0 \tag{9}$$

where

$$\epsilon_b = \begin{Bmatrix} u_{0,x} \\ v_{0,y} \\ u_{0,y} + v_{0,x} \end{Bmatrix} \quad , \quad \epsilon_1 = \begin{Bmatrix} \theta_{x,x} \\ \theta_{y,y} \\ \theta_{x,y} + \theta_{y,x} \end{Bmatrix} \quad , \quad \epsilon_3 = \begin{Bmatrix} \theta_{x,x} + w_{0,xx} \\ \theta_{y,y} + w_{0,yy} \\ \theta_{x,y} + \theta_{y,x} + 2w_{0,xy} \end{Bmatrix} \quad , \quad \gamma_0 = \begin{Bmatrix} \theta_x + w_{0,x} \\ \theta_y + w_{0,y} \end{Bmatrix} \tag{10}$$

The main difference between piezoelectric material and passive materials are in the definition of their constitutive law where for piezoelectric materials, the constitutive law is defined as a set of coupled electromechanical equations as below [11]:

$$\begin{cases} \sigma = Q\epsilon - e^T E \\ D = e\epsilon + kE \end{cases} \tag{11}$$

where the piezoelectric constant matrix e couples the definitions of mechanical stress and electrical displacement vectors. Moreover, in this equation, Q and k are elastic stiffness and dielectric matrices in piezoelectric materials. Considering a plate theory ($\sigma_{zz} = 0$), the components of Equation (11) can be described as follows [39]:

$$\epsilon = \{ \epsilon_b \quad \gamma \}^T \tag{12}$$

$$\sigma = \{ \sigma_b \quad \sigma_s \}^T \quad , \quad \sigma_b = \{ \sigma_{xx} \quad \sigma_{yy} \quad \tau_{xy} \}^T \quad , \quad \sigma_s = \{ \tau_{yz} \quad \tau_{xz} \}^T \tag{13}$$

$$E = -\{ 0 \quad 0 \quad V_z \}^T \tag{14}$$

$$Q = \begin{bmatrix} Q_b & 0 \\ 0 & Q_s \end{bmatrix} \tag{15}$$

$$e = \begin{bmatrix} [e_p]_{3 \times 3} & [e_s]_{3 \times 2} \end{bmatrix} \tag{16}$$

here V_z is the electric potential variation.

3. Meshless Solution

The first step in this numerical solution is the approximation of the displacement field. In this paper, MLS shape functions χ that have a smooth bell-shape variation over the effective domain have been used to approximate the five unknowns of the displacement field introduced in Equation (8) as follows [39,54]:

$$\hat{\mathbf{d}} = [\hat{u}_{0i}, \hat{v}_{0i}, \hat{w}_{0i}, \hat{\theta}_{xi}, \hat{\theta}_{yi}]^T = \sum_{i=1}^n \chi_i d_i \tag{17}$$

where $\hat{\mathbf{d}}$ and \mathbf{d} are the approximated and real values of unknowns over the node numbers n in the effective domain, respectively. The difference between $\hat{\mathbf{d}}$ and \mathbf{d} can be found in [39,54].

Given the meshless form of the approximated values of displacement field (Equation (17)), the strain and electric field vectors can be defined in meshless forms based on approximated displacement and electric potential vectors as follows:

$$\epsilon_b = \{ \xi_0 + z \xi_1 + c_1z^3 \xi_3 \} \hat{\mathbf{d}} \quad , \quad \gamma = (1 + 3c_1z^2) \xi_s \hat{\mathbf{d}} \tag{18}$$

$$E = -\xi_V \hat{V} \tag{19}$$

where

$$\xi_0 = \begin{bmatrix} \chi_{i,x} & 0 & 0 & 0 & 0 \\ 0 & \chi_{i,y} & 0 & 0 & 0 \\ \chi_{i,y} & \chi_{i,x} & 0 & 0 & 0 \end{bmatrix}, \quad \xi_1 = \begin{bmatrix} 0 & 0 & 0 & \chi_{i,x} & 0 \\ 0 & 0 & 0 & 0 & \chi_{i,y} \\ 0 & 0 & 0 & \chi_{i,y} & \chi_{i,x} \end{bmatrix}, \quad \xi_3 = \begin{bmatrix} 0 & 0 & \chi_{i,xx} & \chi_{i,x} & 0 \\ 0 & 0 & \chi_{i,yy} & 0 & \chi_{i,y} \\ 0 & 0 & 2\chi_{i,xy} & \chi_{i,y} & \chi_{i,x} \end{bmatrix} \quad (20)$$

$$\xi_s = \begin{bmatrix} 0 & 0 & \chi_{i,x} & \chi_i & 0 \\ 0 & 0 & \chi_{i,y} & 0 & \chi_i \end{bmatrix}, \quad \xi_v = [0 \quad 0 \quad 1/t_p] \quad (21)$$

By implementing all the meshless forms of vectors and matrices utilized in the weak form (Equation (7)), this equation can be rearranged to determine the governing eigen value equations for the proposed APSs as follows:

$$\mathbf{M}\hat{\mathbf{d}} + \mathbf{K}_{eq}\hat{\mathbf{d}} = 0 \quad (22)$$

where \mathbf{M} and \mathbf{K}_{eq} are the mass and equivalent stiffness matrices which are expressed as:

$$\mathbf{M} = \int_{\Omega} [\xi_0^T \quad \xi_1^T \quad \xi_3^T] \overline{\mathbf{M}} [\xi_0^T \quad \xi_1^T \quad \xi_3^T]^T d\Omega \quad (23)$$

$$\mathbf{K}_{eq} = \mathbf{K}_{uu} + \mathbf{K}_{uv}\mathbf{K}_{vv}^{-1}\mathbf{K}_{vu} \quad (24)$$

in which the pure mechanical \mathbf{K}_{uu} , coupled electromechanical \mathbf{K}_{uv} , and piezoelectric permittivity \mathbf{K}_{vv} stiffness matrices are described as below:

$$\mathbf{K}_{uu} = \int_{\Omega} [\xi_0^T \quad \xi_1^T \quad \xi_3^T] \overline{\mathbf{Q}}_b [\xi_0 \quad \xi_1 \quad \xi_3]^T d\Omega + \int_{\Omega} [\xi_s^T \quad \mathbf{B}_s^T] \overline{\mathbf{Q}}_s [\xi_s \quad \xi_s]^T d\Omega \quad (25)$$

$$\mathbf{K}_{uv} = \mathbf{K}_{vu}^T = \int_{\Omega} [\xi_0^T \quad \xi_1^T \quad \xi_3^T] \overline{\mathbf{E}}_{be} \xi_v d\Omega + \int_{\Omega} [\xi_s^T \quad \xi_s^T] \overline{\mathbf{E}}_{se} \xi_v d\Omega \quad (26)$$

$$\mathbf{K}_{vv} = \int_{\Omega} [\xi_v^T \mathbf{k} \xi_v] d\Omega \quad (27)$$

where $\overline{\mathbf{Q}}$, $\overline{\mathbf{E}}$, $\overline{\mathbf{M}}$ and \mathbf{k} are as follows:

$$\overline{\mathbf{Q}}_b = \int_{-t/2}^{t/2} \begin{bmatrix} 1 & z & c_1 z^3 \\ & z^2 & c_1 z^4 \\ & & c_1^2 z^6 \end{bmatrix} \mathbf{Q}_b dz, \quad \overline{\mathbf{Q}}_s = \int_{-t/2}^{t/2} \begin{bmatrix} 1 & 3c_1 z^2 \\ 3c_1 z^2 & 9c_1^2 z^4 \end{bmatrix} \mathbf{Q}_s dz \quad (28)$$

$$\overline{\mathbf{E}}_{be} = \int_{-t/2}^{t/2} \{1 \quad z \quad c_1 z^3\}^T \mathbf{e}_b dz, \quad \overline{\mathbf{E}}_{se} = \int_{-t/2}^{t/2} \{1 \quad 3c_1 z^2\}^T \mathbf{e}_s dz \quad (29)$$

$$\overline{\mathbf{M}} = \int_{-t/2}^{t/2} \rho \begin{bmatrix} 1 & z & c_1 z^3 \\ & z^2 & c_1 z^4 \\ & & c_1^2 z^6 \end{bmatrix} dz, \quad \mathbf{k} = \int_{-t/2}^{t/2} \mathbf{k} dz \quad (30)$$

4. Results and Discussions

It is assumed that the active layers of the proposed eco-friendly APSs are made of ZnO nanowires placed into a polymeric matrix made of Epoxy. Moreover, the auxetic core layer is made of another polymeric material called PMMA to introduce a lightweight and eco-friendly APS. The electromechanical properties of the utilized polymers and nanowires are as follow:

Epoxy [55,56]: $\rho = 1150 \text{ Kg/m}^3, v = 0.34, E = 3.8 \text{ GPa}, k_{11} = k_{22} = k_{33} = 0.07965 \times 10^{-9} \text{ F/m}$
PMMA [57]: $\rho = 1150 \text{ Kg/m}^3, v = 0.34, E = 2.5 \text{ GPa}$

ZnO NW [58,59]: $Q_{11} = Q_{22} = 209.7$, $Q_{13} = Q_{23} = 105.1$, $Q_{12} = 121.1$ GPa, $Q_{44} = Q_{55} = 42.47$,
 $\rho = 5680$ Kg/m³, $e_{24} = e_{15} = -0.48$ C/m², $e_{31} = e_{32} = -0.573$, $e_{33} = 1.32$,
 $k_{11} = k_{22} = 0.0757 \times 10^{-9}$, $k_{33} = 0.0903 \times 10^{-9}$ F/m

4.1. Validation

Given the novelty of the proposed ASP, there is no reported results for such structures. Therefore, the verification of the developed meshless solution has been confirmed by considering another ASP consisting of a plate made of Aluminum Oxide and sandwich between two active layers of G-1195N piezoceramics. The natural frequencies of such ASP have been reported by Askari et al. [60] and Rouzegar and Abad [61] using an FDST-based Levy's and an HSDT-based Navier's solutions, respectively. Table 1 compares the first five frequencies of this ASP reported by those references with our meshless results. The dimension of this fully simply supported ASP is as $a = b = 400$ mm, $t_c = 5$ mm, and $t_p = 0.1$ mm; this comparison shows our meshless results are between the two other set of natural frequencies which verifies the accuracy our developed method.

Table 1. Natural frequencies (Hz) of a simply supported ASP consisting of a passive layer sandwich between G-1195N piezoceramics.

Reference	1st Mode	2nd Mode	3rd Mode	4th Mode	5th Mode
Rouzegar and Abad [61]	260.03	651.86	651.86	1047.76	1306.58
Askari et al. [60]	265.11	662.20	662.20	1058.59	1322.46
Present	264.09	656.71	657.00	1046.84	1299.86

In addition to the verification of our results with a simplified model, the convergence of the developed meshless solution has also been illustrated in Figure 3. for the eco-friendly ASPs proposed in this paper. In this regard, a cantilever ASP with open-circuit (OC) electrical terminals (as shown in Figure 1), and with $a = b = 0.3$ m, $t_c = 9$ mm; $t_p = 0.5$ mm, $f_0 = 0.4$, $p = 1$, $\alpha_x = 1$, $\beta_x = 0.1$ and $\theta = -45$ has been considered. The variation trend of the obtained frequencies confirms the convergence of the obtained natural frequencies as the curve has no considerable change after using 19 nodes in each direction.

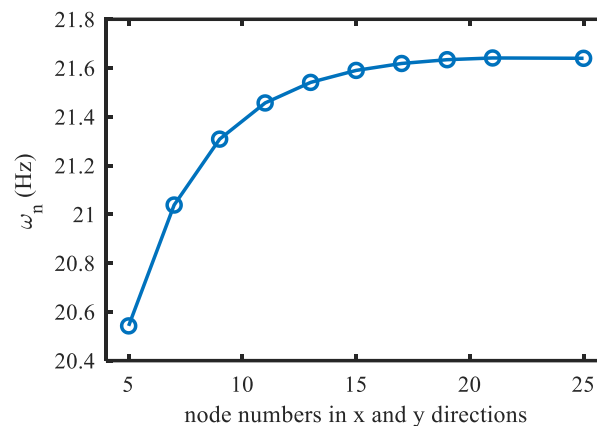


Figure 3. Natural frequency of the eco-friendly APS versus the variation of node numbers.

4.2. Frequencies of the Proposed ASP

This section presents the natural frequency characterization of the eco-friendly ASPs proposed in this paper. In the following simulations, the cantilever ASPs that have been considered for the convergence study have been considered, unless it is mentioned.

Figure 4 illustrates the effects of auxetic unit cell parameters on the natural frequencies of the proposed ASP; this figure shows both cell wall length α_x and slenderness β_x ratios have a significant effect on the natural frequency of ASPs, especially when the core has a negative Poisson's ratio which means $\theta < 0$; it also observed that with the increase in

inclined angle θ which introduces cores with less negative Poisson's ratio, the natural frequency of ASPs is increased. However, when the inclined angle is a positive value, its variation does not considerably affect the natural frequency of the ASPs. Moreover, it can be seen that auxetic cores with higher values of cell wall length α_x and/or lower slenderness β_x ratios offer ASPs with higher natural frequencies. The reason is that the increase in these two parameters in the core leads to ASPs which have higher structural stiffness. Generally speaking, ASPs with an auxetic core have a lower natural frequency in comparison with those with a honeycomb (positive Poisson's ratio) core. Therefore, in ASPs with energy harvester or sensor applications, the use of an auxetic core can be more useful if they are subjected to lower-frequency excitations.

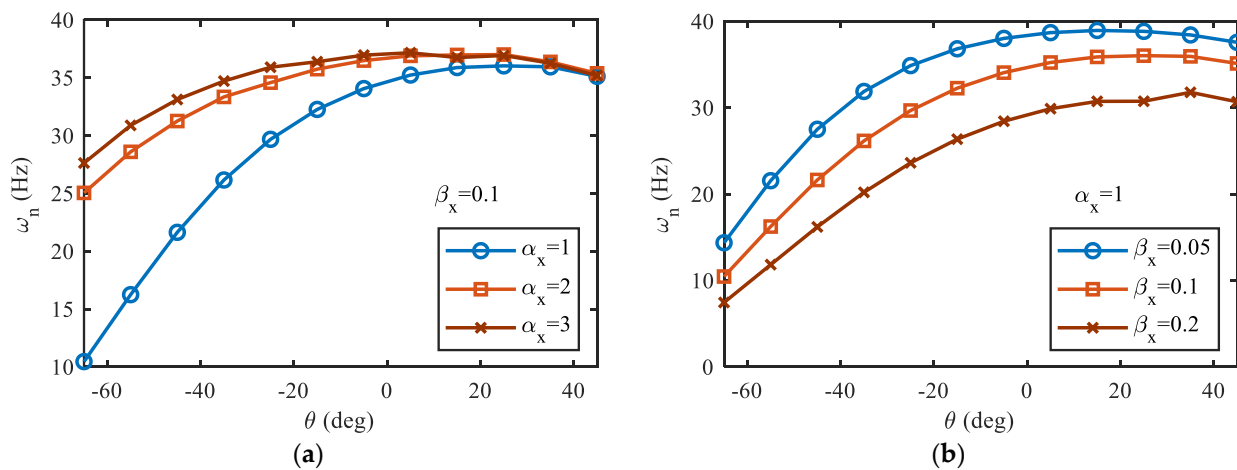


Figure 4. Natural frequency versus inclined angle in core for different (a) cell wall length ratios (b) slenderness ratios in core.

After investigating the auxetic core parameters, Figure 5 explores the effects face sheets' parameters on the frequencies of such ASPs by changing the values nanowire volume fraction f_0 and nanowire distributions p ; this figure reveals that in ASPs with negative values of inclined angle (negative Poisson's ratio), both f_0 and p have a considerable effect on the natural frequencies of the ASPs such that the face sheets with f_0 offers ASPs with higher natural frequencies and p values in face sheets leads to ASPs with lower natural frequencies. However, in ASPs with honeycomb core ($\theta > 0$), these two parameters do not have a significant influence on the frequencies of the proposed ASPs as these types of cores are strong enough to play a considerable role in the structural stiffness of the sandwich plates. Although the existence of ZnO nanowire as the only active component in the proposed ASP is a must, the increase in its volume fraction results in improving the structural stiffness and consequently increasing the natural frequency of the ASP which could have a negative impact on the performance of ASPs when they use as energy harvesters.

The thicknesses of face sheets and core are the other parameters which are investigated in Figures 6 and 7, respectively. Figure 6 shows that increasing the face sheet thickness sharply increases the natural frequency of ASP. Moreover, it shows that lower values of p offer ASPs with higher natural frequencies. Comparing Figure 6b proves that ASPs with higher f_0 have slightly higher natural frequencies. Figure 6 shows that the increase in core thickness also improves the natural frequency of the proposed ASPs at any inclined angles ($\theta > 0$) although this increase is more notable at higher values of cell wall length ratio α_x or lower negative values of inclined angles. In addition, the comparison between Figure 7a,b reveals that auxetic cores with higher values of cell wall length ratio offer ASPs with higher natural frequencies.

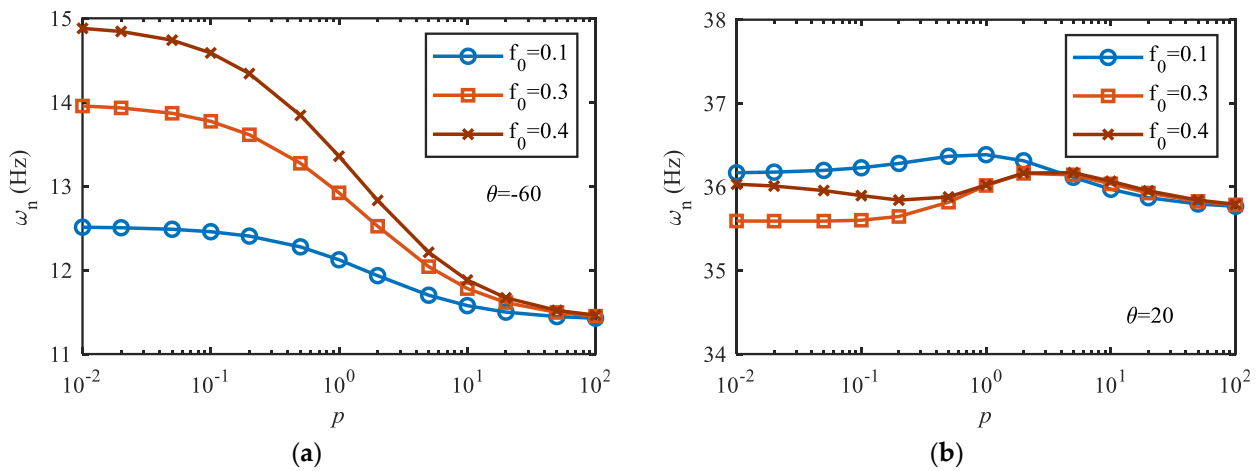


Figure 5. Natural frequency versus nanowire distribution parameter in face sheets for different values nanowire volume fraction at outer faces when the inclined angle is (a) $\theta = -60$, an auxetic core (b) $\theta = 20$, a honeycomb core.

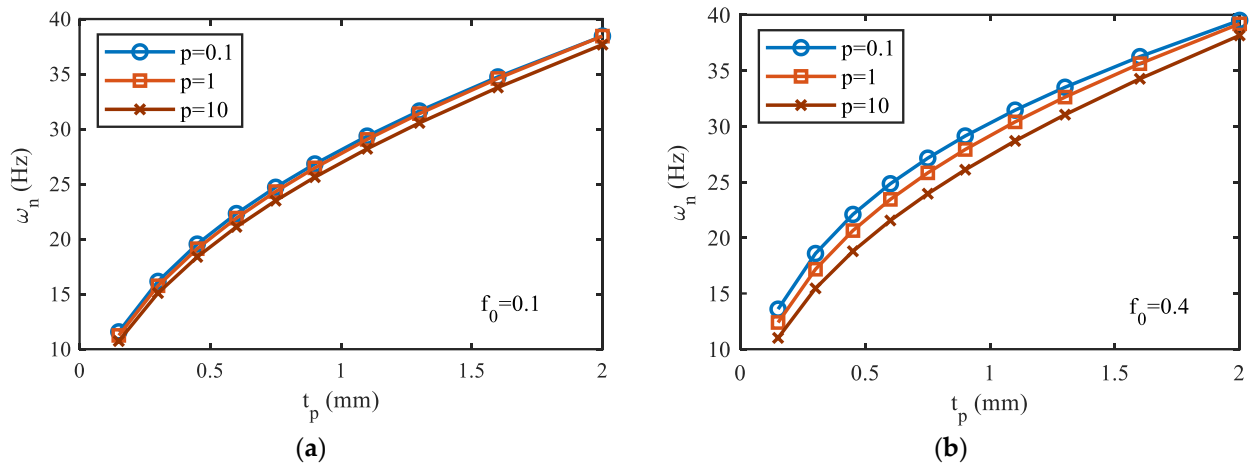


Figure 6. Natural frequency versus thickness of face sheet for different nanowire distribution patterns when (a) $f_0 = 0.1$ (b) $f_0 = 0.4$.

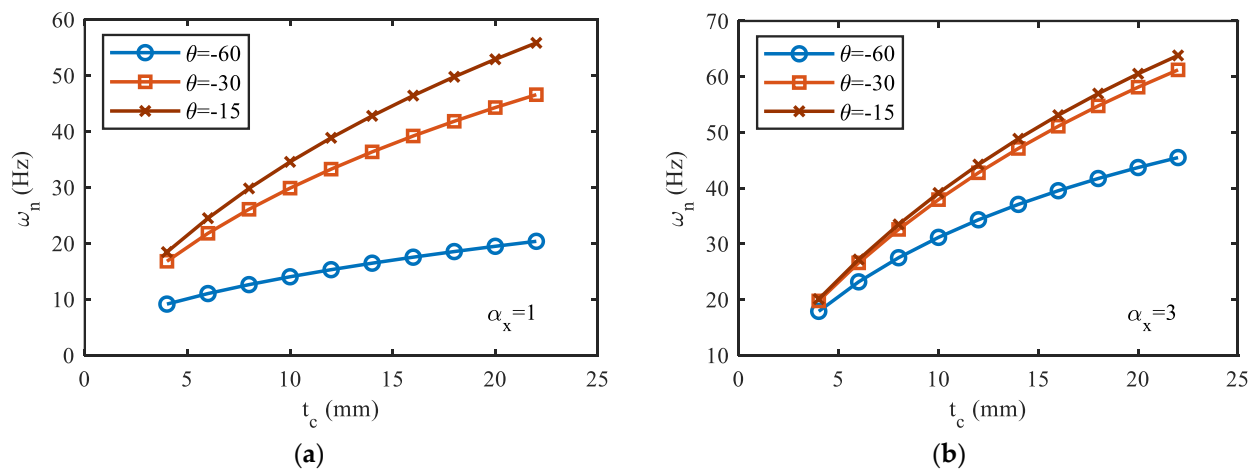


Figure 7. Natural frequency versus thickness of auxetic core for different inclined angles when (a) $\alpha_x = 1$ (b) $\alpha_x = 3$.

Finally, the effect of electrical terminals is investigated on the natural frequencies of proposed ASPs as shown in Table 2; this table lists the natural frequencies of the proposed ASPs with open-circuit and closed-circuit (CC) electrical terminals. Technically the difference between these two electrical terminal set-ups is that in CC both surfaces of the piezoelectric layers are grounded then there would be no piezoelectric effect in ASPs. In other word, CC terminals makes the sandwich plate as a passive structure. The comparison between the natural frequencies of ASPs with OC and CC terminals discloses that the electrical terminal set-up slightly affects the natural frequency of ASPs especially if the amount of the piezoelectric ZnO nanowires is low. Although small differences between the natural frequencies of the same active and passive structures are expected, these very slight differences observed for the proposed ASPs are due to the weak piezoelectric coefficients of the ZnO nanowire/Epoxy nanocomposite used in the face sheets. Moreover, the results listed in this table show that ASPs with higher aspect ratios (a/b) have significantly lower natural frequencies which means that in the design of such structures as an energy harvester, considering a cantilever beam with the same layer arrangement would result in harvesting higher electrical energy out of mechanical displacements.

Table 2. Natural frequencies (Hz) of the proposed ASPs with different electrical terminal set-ups, plate aspect ratio, ZnO nanowire volume fraction and inclined angle when $a = 0.3$ m, $t_c = 9$ mm; $t_p = 0.5$ mm, $p = 1$, $\alpha_x = 1$ and $\beta_x = 0.1$.

θ	Electrical Terminals	$a/b = 0.5$		$a/b = 1$		$a/b = 2$	
		$f_0 = 0.1$	$f_0 = 0.4$	$f_0 = 0.1$	$f_0 = 0.4$	$f_0 = 0.1$	$f_0 = 0.4$
−60	OC	47.843	52.501	12.111	13.348	3.026	3.343
	CC	47.838	52.481	12.110	13.344	3.026	3.342
−30	OC	104.211	108.166	26.797	28.039	6.724	7.059
	CC	104.199	108.128	26.794	28.030	6.723	7.057
−15	OC	121.766	123.115	31.595	32.268	7.948	8.148
	CC	121.752	123.075	31.592	32.258	7.947	8.146

5. Conclusions

In this work, a novel eco-friendly active sandwich plate was introduced to be used as an actuator/sensor or even an energy harvester. The proposed APS was made of an auxetic cantilever plate activated by two piezoelectric layers made of ZnO nanowires and Epoxy. As an important design parameter, the natural frequency of such eco-friendly ASPs was characterized using an in-depth numerical study; this numerical study was based on a developed meshless solution incorporating MLS shape functions and a higher-order plate theory. The following results were concluded:

- ASPs with an auxetic (negative Poisson's ratio) core have much lower natural frequencies in comparison with ASPs with a honeycomb core ($\theta > 0$).
- The increase in cell wall length ratio or the decrease in the slenderness ratio in core layer increases the natural frequency of ASPs.
- The increase in nanowire volume or changing the nanowire distribution pattern considerably affects the natural frequencies of ASPs with an auxetic core.
- According to Table 2, it is expected that the proposed ASP would be weaker than structures that are activated with traditional piezoceramics in terms of electrical-mechanical energy conversion, although the proposed ASP is an eco-friendly and bio-compatible structure.
- Furthermore, the effect of the electrical terminal set-up on the natural frequencies was found insignificant. Nevertheless, the electrical terminal set-up plays a crucial role in the electrical functionality of the device.
- Another concern of the proposed ASP is some manufacturing limitations associated with auxetic core, which mainly needs to be 3D-printed.

Author Contributions: Formal analysis, R.M.-D. and K.B.; Investigation, R.M.-D.; Methodology, R.M.-D., Project administration, K.B.; Software, R.M.-D., Supervision, K.B.; Validation, R.M.-D.; Visualization, R.M.-D. and K.B.; Writing—original draft, R.M.-D.; Writing—review and editing, R.M.-D. and K.B. All authors have read and agreed to the published version of the manuscript.

Funding: This research was funded by the Connaught Grant Challenge Awards for Energy Harvesting in Biomedical Applications and NSERC of Canada (under grant number RGPIN-217525).

Institutional Review Board Statement: Not applicable.

Informed Consent Statement: Not applicable.

Data Availability Statement: Not applicable.

Acknowledgments: This research was supported by the Connaught Grant Challenge Awards for Energy Harvesting in Biomedical Applications and NSERC of Canada (under grant number RGPIN-217525). The authors are grateful for their support.

Conflicts of Interest: The authors declare no conflict of interest. The funders had no role in the design of the study; in the collection, analyses, or interpretation of data; in the writing of the manuscript; or in the decision to publish the results.

References

1. Kundalwal, S.I.; Ray, M.C. Smart Damping of Fuzzy Fiber Reinforced Composite Plates Using 1-3 Piezoelectric Composites. *J. Vib. Control* **2016**, *22*, 1526–1546. [[CrossRef](#)]
2. Liang, H.; Hao, G.; Olszewski, O.Z. A Review on Vibration-Based Piezoelectric Energy Harvesting from the Aspect of Compliant Mechanisms. *Sens. Actuators A Phys.* **2021**, *331*, 112743. [[CrossRef](#)]
3. Yang, Z.; Zhou, S.; Zu, J.; Inman, D. High-Performance Piezoelectric Energy Harvesters and Their Applications. *Joule* **2018**, *2*, 642–697. [[CrossRef](#)]
4. Grilli, L.; Casset, F.; Bressy, C.; Brisset, H.; Briand, J.-F.; Barry-Martinet, R.; Colin, M. Development, Optimization, Biological Assays, and In Situ Field Immersion of a Transparent Piezoelectric Vibrating System for Antifouling Applications. *Actuators* **2022**, *11*, 47. [[CrossRef](#)]
5. Sezer, N.; Koç, M. A Comprehensive Review on the State-of-the-Art of Piezoelectric Energy Harvesting. *Nano Energy* **2021**, *80*, 105567. [[CrossRef](#)]
6. Liu, L.; Guo, X.; Lee, C. Promoting Smart Cities into the 5G Era with Multi-Field Internet of Things (IoT) Applications Powered with Advanced Mechanical Energy Harvesters. *Nano Energy* **2021**, *88*, 106304. [[CrossRef](#)]
7. Zhao, Z.; Dai, Y.; Dou, S.X.; Liang, J. Flexible Nanogenerators for Wearable Electronic Applications Based on Piezoelectric Materials. *Mater. Today Energy* **2021**, *20*. [[CrossRef](#)]
8. Sharma, S.; Vig, R.; Kumar, N. Finite Element Modeling of Smart Piezo Structure: Considering Dependence of Piezoelectric Coefficients on Electric Field. *Mech. Based Des. Struct. Mach.* **2016**, *44*, 372–383. [[CrossRef](#)]
9. Krishnaswamy, J.A.; Buroni, F.C.; Garcia-Sanchez, F.; Melnik, R.; Rodriguez-Tembleque, L.; Saez, A. Lead-Free Piezocomposites with CNT-Modified Matrices: Accounting for Agglomerations and Molecular Defects. *Compos. Struct.* **2019**, *224*, 111033. [[CrossRef](#)]
10. Tan, P.; Tong, L. Micro-Electromechanics Models for Piezoelectric-Fiber-Reinforced Composite Materials. *Compos. Sci. Technol.* **2001**, *61*, 759–769. [[CrossRef](#)]
11. Mosallaie Barzoki, A.A.; Ghorbanpour Arani, A.; Kolahchi, R.; Mozdianfard, M.R. Electro-Thermo-Mechanical Torsional Buckling of a Piezoelectric Polymeric Cylindrical Shell Reinforced by DWBNNTs with an Elastic Core. *Appl. Math. Model.* **2012**, *36*, 2983–2995. [[CrossRef](#)]
12. Fan, Z.; Mo, X.; Lou, C.; Yao, Y.; Wang, D.; Chen, G.; Lu, J.G. Structures and Electrical Properties of Ag-Tetracyanoquinodimethane Organometallic Nanowires. *Nanotechnol. IEEE Trans.* **2005**, *4*, 238–241. [[CrossRef](#)]
13. Qin, Y.; Wang, X.; Wang, Z.L. Microfibre-Nanowire Hybrid Structure for Energy Scavenging. *Nature* **2008**, *451*, 809–814. [[CrossRef](#)] [[PubMed](#)]
14. Wang, Z.L.; Song, J. Piezoelectric Nanogenerators Based on Zinc Oxide Nanowire Arrays. *Science* **2006**, *312*, 242–246. [[PubMed](#)]
15. Momeni, K. A Multiscale Approach to Nanocomposite Electrical Generators. *Nano Energy* **2014**, *4*, 132–139. [[CrossRef](#)]
16. Saravanakumar, B.; Thiyagarajan, K.; Alluri, N.R.; SoYoon, S.; Taehyun, K.; Lin, Z.H.; Kim, S.J. Fabrication of an Eco-Friendly Composite Nanogenerator for Self-Powered Photosensor Applications. *Carbon N. Y.* **2015**, *84*, 56–65. [[CrossRef](#)]
17. Moradi-Dastjerdi, R.; Behdinin, K. Dynamic Performance of Piezoelectric Energy Harvesters with a Multifunctional Nanocomposite Substrate. *Appl. Energy* **2021**, *293*, 116947. [[CrossRef](#)]
18. Setoodeh, A.R.; Shojaee, M.; Malekzadeh, P. Application of Transformed Differential Quadrature to Free Vibration Analysis of FG-CNTRC Quadrilateral Spherical Panel with Piezoelectric Layers. *Comput. Methods Appl. Mech. Engrg.* **2018**, *335*, 510–537. [[CrossRef](#)]

19. Zhang, J.; Zhang, J.; Shu, C.; Fang, Z. Enhanced Piezoelectric Wind Energy Harvesting Based on a Buckled Beam. *Appl. Phys. Lett.* **2017**, *110*, 183903. [[CrossRef](#)]
20. Ansari, M.H.; Karami, M.A. Energy Harvesting from Controlled Buckling of Piezoelectric Beams. *Smart Mater. Struct.* **2015**, *24*, 115005. [[CrossRef](#)]
21. Malekzadeh, P.; Setoodeh, A.R.; Shojaee, M. Vibration of FG-GPLs Eccentric Annular Plates Embedded in Piezoelectric Layers Using a Transformed Differential Quadrature Method. *Comput. Methods Appl. Mech. Eng.* **2018**, *340*, 451–479. [[CrossRef](#)]
22. Sobhani, E.; Masoodi, A.R. Natural Frequency Responses of Hybrid Polymer/Carbon Fiber/FG-GNP Nanocomposites Paraboloidal and Hyperboloidal Shells Based on Multiscale Approaches. *Aerosp. Sci. Technol.* **2021**, *119*, 107111. [[CrossRef](#)]
23. Liu, Y.; Hu, W.; Zhu, R.; Safaei, B.; Qin, Z.; Chu, F. Dynamic Responses of Corrugated Cylindrical Shells Subjected to Nonlinear Low-Velocity Impact. *Aerosp. Sci. Technol.* **2022**, *121*, 107321. [[CrossRef](#)]
24. Sheikh, T.; Behdinin, K. Multiscale Analysis of Laminates Printed by 3D Printing Fused Deposition Modeling Method. *Adv. Compos. Mater. Struct.* **2022**, 233–243. [[CrossRef](#)]
25. Sobhani, E.; Masoodi, A.R.; Ahmadi-Pari, A.R. Vibration of FG-CNT and FG-GNP Sandwich Composite Coupled Conical-Cylindrical-Conical Shell. *Compos. Struct.* **2021**, *273*, 114281. [[CrossRef](#)]
26. Sobhani, E.; Arbabian, A.; Civalek, Ö. The Free Vibration Analysis of Hybrid Porous Nanocomposite Joined Hemispherical-Cylindrical-Conical Shells. *Eng. Comput.* **2021**. [[CrossRef](#)]
27. Trivedi, N.; Das, S.; Craciun, E.-M. The Mathematical Study of an Edge Crack in Two Different Specified Models under Time-Harmonic Wave Disturbance. *Mech. Compos. Mater.* **2022**. [[CrossRef](#)]
28. Alian, A.R.; Meguid, S.A.; Kundalwal, S.I. Unraveling the Influence of Grain Boundaries on the Mechanical Properties of Polycrystalline Carbon Nanotubes. *Carbon N. Y.* **2017**, *125*, 180–188. [[CrossRef](#)]
29. Moradi-Dastjerdi, R.; Behdinin, K. Stress Waves in Thick Porous Graphene-Reinforced Cylinders under Thermal Gradient Environments. *Aerosp. Sci. Technol.* **2021**, *110*, 106476. [[CrossRef](#)]
30. Ghahramani, P.; Behdinin, K.; Moradi-Dastjerdi, R.; Naguib, H.E. Theoretical and Experimental Investigation of MWCNT Dispersion Effect on the Elastic Modulus of Flexible PDMS / MWCNT Nanocomposites. *Nanotechnol. Rev.* **2022**, *11*, 55–64. [[CrossRef](#)]
31. Yasin Alibar, M.; Safaei, B.; Asmael, M.; Zeeshan, Q. Effect of Carbon Nanotubes and Porosity on Vibrational Behavior of Nanocomposite Structures: A Review. *Arch. Comput. Methods Eng.* **2022**, *29*, 2621–2657. [[CrossRef](#)]
32. Pan, S.; Feng, J.; Safaei, B.; Qin, Z.; Chu, F.; Hui, D. A Comparative Experimental Study on Damping Properties of Epoxy Nanocomposite Beams Reinforced with Carbon Nanotubes and Graphene Nanoplatelets. *Nanotechnol. Rev.* **2022**, *11*, 1658–1669. [[CrossRef](#)]
33. Chang, E.; Ameli, A.; Alian, A.R.; Mark, L.H.; Yu, K.; Wang, S.; Park, C.B. Percolation Mechanism and Effective Conductivity of Mechanically Deformed 3-Dimensional Composite Networks: Computational Modeling and Experimental Verification. *Compos. Part B Eng.* **2021**, *207*, 108552. [[CrossRef](#)]
34. Nuhu, A.A.; Safaei, B. A Comprehensive Review on the Vibration Analyses of Small-Scaled Plate-Based Structures by Utilizing the Nonclassical Continuum Elasticity Theories. *Thin-Walled Struct.* **2022**, *179*, 109622. [[CrossRef](#)]
35. Moradi-Dastjerdi, R.; Meguid, S.A.; Rashahmadi, S. Electro-Dynamic Analysis of Smart Nanoclay-Reinforced Plates with Integrated Piezoelectric Layers. *Appl. Math. Model.* **2019**, *75*, 267–278. [[CrossRef](#)]
36. Moradi-Dastjerdi, R.; Malek-Mohammadi, H.; Momeni-Khabisi, H. Free Vibration Analysis of Nanocomposite Sandwich Plates Reinforced with CNT Aggregates. *ZAMM-J. Appl. Math. Mech./Zeitschrift für Angew. Math. Mech.* **2017**, *97*, 1418–1435. [[CrossRef](#)]
37. Sobhani, E.; Masoodi, A.R.; Civalek, O.; Ahmadi-Pari, A.R. Agglomerated Impact of CNT vs. GNP Nanofillers on Hybridization of Polymer Matrix for Vibration of Coupled Hemispherical-Conical-Conical Shells. *Aerosp. Sci. Technol.* **2022**, *120*, 107257. [[CrossRef](#)]
38. Moradi-Dastjerdi, R.; Rashahmadi, S.; Meguid, S.A. Electro-Mechanical Performance of Smart Piezoelectric Nanocomposite Plates Reinforced by Zinc Oxide and Gallium Nitride Nanowires. *Mech. Based Des. Struct. Mach.* **2022**, *50*, 1954–1967. [[CrossRef](#)]
39. Moradi-Dastjerdi, R.; Behdinin, K. Biaxial Buckling Analysis of an Innovative Active Sandwich Plate. *Mech. Based Des. Struct. Mach.* **2022**, 1–14. [[CrossRef](#)]
40. Behdinin, K.; Moradi-Dastjerdi, R. Thermal Buckling Resistance of a Lightweight Lead-Free Piezoelectric Nanocomposite Sandwich Plate. *Adv. Nano Res.* **2022**, *12*, 593–603.
41. De Bellis, M.L.; Bacigalupo, A.; Zavarise, G. Characterization of Hybrid Piezoelectric Nanogenerators through Asymptotic Homogenization. *Comput. Methods Appl. Mech. Eng.* **2019**, *355*, 1148–1186. [[CrossRef](#)]
42. Choi, M.; Murillo, G.; Hwang, S.; Kim, J.W.; Jung, J.H.; Chen, C.Y.; Lee, M. Mechanical and Electrical Characterization of PVDF-ZnO Hybrid Structure for Application to Nanogenerator. *Nano Energy* **2017**, *33*, 462–468. [[CrossRef](#)]
43. Arshid, E.; Amir, S.; Loghman, A. Bending and Buckling Behaviors of Heterogeneous Temperature-Dependent Micro Annular/Circular Porous Sandwich Plates Integrated by FGPEM Nano-Composite Layers. *J. Sandw. Struct. Mater.* **2021**, *23*, 3836–3877. [[CrossRef](#)]
44. Hu, C.; Behdinin, K.; Moradi-Dastjerdi, R. PVDF Energy Harvester for Prolonging the Battery Life of Cardiac Pacemakers. *Actuators* **2022**, *11*, 187. [[CrossRef](#)]
45. Kim, J.; Byun, S.; Lee, S.; Ryu, J.; Cho, S.; Oh, C.; Kim, H.; No, K.; Ryu, S.; Lee, Y.M.; et al. Cost-Effective and Strongly Integrated Fabric-Based Wearable Piezoelectric Energy Harvester. *Nano Energy* **2020**, *75*, 104992. [[CrossRef](#)]

46. Angelou, A.; Norman, C.; Miran, N.; Albers, S.; Moradi-Dastjerdi, R.; Behdinan, K. An Eco-Friendly, Biocompatible and Reliable Piezoelectric Nanocomposite Actuator for the New Generation of Microelectronic Devices. *Eur. Phys. J. Plus* **2021**, *136*, 678. [[CrossRef](#)]
47. Zhao, X.; Shang, Z.; Luo, G.; Deng, L. A Vibration Energy Harvester Using AlN Piezoelectric Cantilever Array. *Microelectron. Eng.* **2015**, *142*, 47–51. [[CrossRef](#)]
48. Elfrink, R.; Kamel, T.M.; Goedbloed, M.; Matova, S.; Hohlfeld, D.; van Andel, Y.; van Schaijk, R. Vibration Energy Harvesting with Aluminum Nitride-Based Piezoelectric Devices. *J. Micromech. Microeng* **2009**, *19*, 94005. [[CrossRef](#)]
49. Meschino, M.; Wang, L.; Xu, H.; Moradi-Dastjerdi, R.; Behdinan, K. Low-Frequency Nanocomposite Piezoelectric Energy Harvester with Embedded Zinc Oxide Nanowires. *Polym. Compos.* **2021**, *42*, 4573–4585. [[CrossRef](#)]
50. Duc, N.D.; Cong, P.H. Nonlinear Dynamic Response and Vibration of Sandwich Composite Plates with Negative Poisson's Ratio in Auxetic Honeycombs. *J. Sandw. Struct. Mater.* **2018**, *20*, 692–717. [[CrossRef](#)]
51. Moradi-Dastjerdi, R.; Behdinan, K. Thermo-Electro-Mechanical Behavior of an Advanced Smart Lightweight Sandwich Plate. *Aerosp. Sci. Technol.* **2020**, *106*, 106142. [[CrossRef](#)]
52. Tran, L.V.; Thai, C.H.; Nguyen-xuan, H. An Isogeometric Finite Element Formulation for Thermal Buckling Analysis of Functionally Graded Plates. *Finite Elem. Anal. Des.* **2013**, *73*, 65–76. [[CrossRef](#)]
53. Reddy, J.N. *Mechanics of Laminated Composite Plates and Shells: Theory and Analysis*; CRC Press: Boca Raton, FL, USA, 2004; ISBN 0849315921.
54. Lancaster, P.; Salkauskas, K. Surface Generated by Moving Least Squares Methods. *Math. Comput.* **1981**, *37*, 141–158. [[CrossRef](#)]
55. Yasmin, A.; Luo, J.J.; Abot, J.L.; Daniel, I.M. Mechanical and Thermal Behavior of Clay/Epoxy Nanocomposites. *Compos. Sci. Technol.* **2006**, *66*, 2415–2422. [[CrossRef](#)]
56. Berger, H.; Kari, S.; Gabbert, U.; Rodriguez-Ramos, R.; Guinovart, R.; Otero, J.A.; Bravo-Castillero, J. An Analytical and Numerical Approach for Calculating Effective Material Coefficients of Piezoelectric Fiber Composites. *Int. J. Solids Struct.* **2005**, *42*, 5692–5714. [[CrossRef](#)]
57. Shen, H.-S. Postbuckling of Nanotube-Reinforced Composite Cylindrical Shells in Thermal Environments, Part I: Axially-Loaded Shells. *Compos. Struct.* **2011**, *93*, 2096–2108. [[CrossRef](#)]
58. Mishra, N.; Krishna, B.; Singh, R.; Das, K. Evaluation of Effective Elastic, Piezoelectric, and Dielectric Properties of SU8/ZnO Nanocomposite for Vertically Integrated Nanogenerators Using Finite Element Method. *J. Nanomater.* **2017**, *2017*, 1924651. [[CrossRef](#)]
59. Özgür, Ü.; Alivov, Y.I.; Liu, C.; Teke, A.; Reshchikov, M.A.; Doğan, S.; Avrutin, V.; Cho, S.J.; Morkç, H. A Comprehensive Review of ZnO Materials and Devices. *J. Appl. Phys.* **2005**, *98*, 41301. [[CrossRef](#)]
60. Askari Farsangi, M.A.; Saidi, A.R. Levy Type Solution for Free Vibration Analysis of Functionally Graded Rectangular Plates with Piezoelectric Layers. *Smart Mater. Struct.* **2012**, *21*, 94017. [[CrossRef](#)]
61. Rouzegar, J.; Abad, F. Free Vibration Analysis of FG Plate with Piezoelectric Layers Using Four-Variable Refined Plate Theory. *Thin-Walled Struct.* **2015**, *89*, 76–83. [[CrossRef](#)]